Journal of Vacuum Science and Technology A

RESEARCH ARTICLE | APRIL 07 2025

Molecular beam epitaxy of boron arsenide layers

Special Collection: Molecular Beam Epitaxy

Tin S. Cheng ; Jonathan Bradford ; Leo Norman ; Xiaoyang Ji ; Arpit Nandi ;
Gerardo T. Martinez ; Stuart Robertson ; Paul R. Edwards ; James W. Pomeroy ; David Cherns ;
Christopher J. Mellor ; Robert W. Martin ; Peter H. Beton ; Martin Kuball ; Sergei V. Novikov ✉

Check for updates

J. Vac. Sci. Technol. A 43, 032705 (2025)
https://doi.org/10.1116/6.0004383

View Online

Export Citation

JVST A
Journal of Vacuum Science & Technology A
ARTICLE
pubs.aip.org/avs/jva

Molecular beam epitaxy of boron arsenide layers

Cite as: J. Vac. Sci. Technol. A **43**, 032705 (2025); doi: 10.1116/6.0004383
Submitted: 10 January 2025 · Accepted: 19 March 2025 ·
Published Online: 7 April 2025

View Online
Export Citation
CrossMark

Tin S. Cheng,[1] Jonathan Bradford,[1] Leo Norman,[2] Xiaoyang Ji,[2] Arpit Nandi,[2] Gerardo T. Martinez,[3] Stuart Robertson,[4] Paul R. Edwards,[5] James W. Pomeroy,[2] David Cherns,[2] Christopher J. Mellor,[1] Robert W. Martin,[5] Peter H. Beton,[1] Martin Kuball,[2] and Sergei V. Novikov[1,a)]

AFFILIATIONS

[1] School of Physics and Astronomy, University of Nottingham, Nottingham NG7 2RD, United Kingdom
[2] Center for Device Thermography and Reliability, University of Bristol, Tyndall Avenue, Bristol BS8 1TL, United Kingdom
[3] Department of Materials, University of Oxford, Oxford OX1 2JD, United Kingdom
[4] Loughborough Materials Characterisation Centre, Loughborough University, Loughborough LE11 3TU, United Kingdom
[5] Department of Physics, SUPA, University of Strathclyde, Glasgow G4 0NG, United Kingdom

Note: This paper is a part of the Special Topic Collection on Molecular Beam Epitaxy.

[a)] **Author to whom correspondence should be addressed:** Sergei.Novikov@nottingham.ac.uk

ABSTRACT

Thermal management is the main technological challenge for next generation electronic devices. Recently, several groups successfully demonstrated boron arsenide (BAs) microcrystals with an ultrahigh thermal conductivity approaching that of diamond. The development of scalable epitaxial BAs growth techniques is urgently required to enable a transition of BAs material to real applications. We have grown boron arsenide layers on 3C-SiC/Si and sapphire substrates over a wide temperature range using molecular beam epitaxy (MBE). We have confirmed the incorporation of arsenic by a wide range of characterization techniques. The best quality of the boron arsenide layers was achieved at high growth temperatures of around 750 °C. We have demonstrated that high temperatures nucleation of the boron arsenide layer started with deposition of boron-rich monolayers on the substrate surface. For the epitaxy on sapphire during the initial growth phase, the cubic boron arsenide layers align with the hexagonal structure of the sapphire substrate and grow in the $\langle 111 \rangle$ direction for a few crystalline monolayers; however, currently, we are not able to sustain that, and the boron arsenide layer becomes amorphous. For boron arsenide layers grown at high temperatures, we have observed an increase in the thermal conductivity and cathodoluminescence optical response with a reproducible peak centered at ∼1.67 eV. The experimental results are explained by increased chemical interaction between arsenic and boron at growth temperatures above ∼600 °C. Our experimental data show that MBE growth conditions need to be further optimized first to improve stoichiometry and after that to decrease point-defect densities in boron arsenide layers to achieve an increase in the thermal conductivity.

I. INTRODUCTION

Thermal management and heat dissipation has become the main technological challenge for the next generation of electronic devices as excessive temperature rise results in degradation of device performance and early failure of devices. Miniaturization is the main trend for all electronics, with Moore's law predicting that the number of transistors on an integrated circuit doubles about every two years. Heat generated by any device must be effectively dissipated to improve performance, reliability, and prevent premature failures. With all electronic devices becoming smaller, the challenge of thermal management has become one of the major problems preventing further miniaturization.

There are a limited number of materials with sufficiently high thermal conductivity for passive cooling of electronic devices, which are cost-effective and reliable. The ideal material is diamond with a thermal conductivity as large as 2300 W/m K,[1,2] but it is costly to produce, in particular, single-crystalline material in sufficient quantity. This has limited the use of diamond in electronic applications so far;[3] therefore, copper (∼400 W/m K)[4] and aluminum (∼200 W/m K)[4] remain the most widely used materials for heat dissipation in current electronic devices.

According to early theoretical predictions, boron arsenide (BAs) was not considered as a potential material for heat dissipation.[5] Interest in BAs, however, was reignited by more recent theoretical calculations, which suggested that BAs has an ultrahigh thermal conductivity comparable to that of diamond.[6] The difference in boron and arsenic masses produces an energy gap between the optical and acoustic phonons in BAs, which results in a decrease in phonon scattering, more efficient phonon transport through the material and, therefore, high thermal conductivity. Theoretical studies suggest a very high value of ∼1400 W/m K.[7] However, the first experimental attempts to confirm the ultrahigh thermal conductivity of boron arsenide failed. The structural quality of the available bulk BAs material was not good enough and point-defect scattering limited the thermal conductivity to only 200 W/m K.[8] In 2018, three groups independently reported the growth of BAs microcrystals with thermal conductivities in the range of 900–1300 W/m K.[9–11] All three groups observed that in order to improve thermal conductivity, they had to drastically decrease the defect density concentration.[9–11] They achieved BAs microcrystals with sizes ranging from 0.5 to 2 mm after growth times of several weeks.[9–11] However, these BAs microcrystals are too small for any practical applications. Only the development of an epitaxial growth technique over large areas will enable a true translation of BAs to real-life applications.

It has been demonstrated[12] that even small high-quality BAs-microcrystal cooling substrates allow substantially lower hot-spot temperatures to be exhibited in prototype GaN transistors due to their unique phonon band structures and interface matching beyond those when using diamond and silicon carbide substrates. This illustrates the high potential for using BAs in the thermal management of radiofrequency electronics. However, currently available BAs crystals are only a few millimeter in size.

It was theoretically predicted that zinc-blende BAs can potentially have simultaneously both high hole mobility (2110 cm^2/V s) and high electron mobility (1400 cm^2/V s) at room temperature,[13] which is very rare in semiconductors. Therefore, binary BAs is not only attractive for passive cooling of electronics such as for GaN devices, but also a very promising novel material that may be transformative for electronic and photovoltaic devices, though its Baliga figure of merit may not be that high considering the lower bandgap.

BAs has a zinc-blende (cubic) crystal structure with a lattice parameter of ∼0.48 nm[8,14] and is a semiconductor with a bandgap of ∼1.5 eV.[10,14] Zinc-blende BAs is stable up to temperatures of about 920 °C and undergoes irreversible decomposition to icosahedral subarsenides $B_{13}As_2$ or $B_{12}As_2$ at higher temperatures.[14–18] The high volatility of arsenic results in a high density of point defects and vacancies in BAs crystals.

As the growth temperatures for zinc-blende BAs needs to be below 920 °C, molecular beam epitaxy (MBE) will have some potential advantage for a scalable approach to produce BAs layers, as a well-known low-temperature growth technique in comparison to high-temperature chemical vapor deposition or metal-organic chemical vapor deposition (MOCVD).

The formation of BAs compound by the direct reaction of B and As was first achieved in 1958 at relatively high temperatures of 800 °C.[18] At the same time, it was reported that a growth temperature of 920 °C should not be exceeded to avoid the irreversible formation of $B_{12}As_2$.[18] It was also reported that irreversible thermal decomposition of BAs was observed for temperatures above 850 °C.[14,19,20] It was theoretically predicted that the BAs enthalpy is nearly zero at 1000 K (727 °C) and at the formation of BAs becomes endothermic above this temperature.[20] Recently, it was demonstrated that the preferred growth temperature range for successful chemical vapor transport (CVT) of BAs microcrystals is between 727 and 920 °C (Refs. 9–11 and 21 and references therein). However, it is well established that in MBE arsenic will actively desorb from the substrate surfaces at temperatures above 650–700 °C.[22]

The aim of this study is to explore the feasibility of scalable MBE technology for the growth of boron arsenide layers and to study their properties by a wide range of characterization techniques.

II. EXPERIMENT

We have studied MBE growth of BAs layers using a Veeco MOD-GENII system. The MBE system can achieve growth temperatures of up to 950 °C and is capable of growth on rotating substrates of up to 3 in. in diameter. We are using a high-temperature sublimation Veeco source for boron. Boron has two naturally occurring stable isotopes and the natural mixture contains ^{11}B (80.1%) and ^{10}B (19.9%). In this study, we have used isotopically enriched (>98%) boron ^{11}B with 6 N purity. Beam flux measurements for high-temperature boron source are not reliable and so consistent with our previous studies, we used thermocouple readings to control the temperature of the boron cell.[23–26] We quote the temperatures of the boron cell, but not the boron beam equivalent pressures (BEPs), because we were not able to achieve reliable measurements of the boron flux with the beam monitoring ion gauge. At extremely high source temperatures above 1600 °C, the boron source produces not only a flux of boron, but also a flux of nitrogen, due to the start of sublimation of the pyrolytic boron nitride components of the cell. Arsenic in the form of As_2 or As_4 is produced by a valved Veeco cracker allowing us to explore the growth of BAs layers using arsenic fluxes with different chemical reactivity. In all experiments in this study, we have used As_2 fluxes to increase arsenic reactivity.

The choice of substrates will be crucial to achieve low defects and dislocation densities in the BAs layers. Ideally, we need to grow BAs on the native lattice matched BAs bulk substrates. However, the maximum size of the current bulk BAs microcrystals is less than a few millimeters.[9–11] Commercially, available zinc-blende (cubic) silicon carbide 3C-SiC substrates with a lattice constant of 0.44 nm are the closest lattice to the BAs layers [0.48 nm (Refs. 9–11)]. In our research, we have used cubic 3C-SiC templates grown on Si (Novasic). Three-in. diameter 3C-SiC templates were diced to 10 × 10 mm^2 wafers to reduce our costs. We have also used widely available 2-in. diameter (0001) sapphire substrates. Even if the growth conditions for two types of the wafers may be identical, BAs layers will be growing on them at slightly different conditions. We used thermocouple readings to control the temperature of the growth surface. When comparing experimental data, we must remember that real temperatures of the substrate surface for 10 × 10 mm^2 3C-SiC wafers will be different from the temperature of 2-in. diameter sapphire at the same thermocouple readings due to the different design of the 3-in. diameter substrate holders, different thermal coupling, and different optical properties of these two substrates.

The MBE growth of BAs layers on different substrates was investigated using *in situ* reflection high-energy electron diffraction (RHEED) and *ex situ* structural techniques including atomic force microscope (AFM), scanning electron microscopy (SEM), variable angle spectroscopic ellipsometry (VASE), x-ray photoelectron spectroscopy (XPS), secondary ion mass spectrometry (SIMS), and transmission electron microscopy (TEM).

Topographic images of the BAs layers were acquired by AFM after growth with amplitude-modulated tapping mode atomic force microscopy AC-AFM, in ambient conditions with an Asylum Research Cypher-S AFM using SCOUO70Al probes (NuNano, stiffness ∼2 N/m) cantilevers. AFM image processing and analysis was performed using GWYDDION.[27]

VASE was performed using a M2000-DI instrument produced by J. A. Woollam Inc. The results were collected over a wide wavelength range from 1690 to 192 nm using focusing probes, with an elliptical spot with a minor axis of 200 μm; the major axis of the ellipse depends on the angles of incidence. The results were analyzed using COMPLETEEASE®software version 6.73.

The chemical concentrations of B and As elements were studied as a function of depth using SIMS in two commercial systems, a Cameca IMS-3F and a Cameca IMS-7F systems. The arsenic analysis was carried out using Cs^+ primary ion bombardment and negative secondary ion detection to optimize sensitivity to the elements of interest. The boron analysis was carried out using O_2^+ primary ion bombardment and positive secondary ion detection to optimize sensitivity to boron. The data were not quantified due to a lack of suitable reference calibration standards.

Wavelength-dispersive x-ray spectroscopy (WDX) was used to obtain elemental information about surface composition using a JEOL 8530F electron probe microanalyzer. Electron beam voltages of 5 and 10 kV were used with the electron current set at values in the 1–10 nA range. The samples were mounted using a highly conductive silver paint but were still prone to charging such that the voltages mentioned above are offset by several kV of charging at the sample surface.

XPS was measured using a Kratos Axis Ultra DLD instrument equipped with a monochromated Al K_α x-ray source ($h\nu = 1486.7$ eV) operated at 15 kV and 10 mA. Survey spectra were recorded at pass energy of 160 eV and high-resolution core level spectra were measured at 20 eV pass energy. Charge compensation was provided by flooding the surface with 3.5 eV electrons. XPS data were analyzed using the CASAXPS software package.[28] The binding energy scale was calibrated by a rigid shift of the spectra to align the C 1s peak of adventitious carbon to 285 eV.

Structural properties of thicker BAs layers have been studied using high-resolution transmission electron microscopy (HRTEM) and scanning transmission electron microscopy with high angle annular dark-field (HAADF-STEM). Cross-sectional lamella of BAs/sapphire samples were produced by ThermoFisher Scios 2 DualBeam focused ion beam milling. A 30 kV, 30 nA and 30 kV, 15 nA chunk cutting sequence was used, followed by cleaning at 30 kV, 3 nA and 30 kV, 50 pA, thinning of the lamellae at 30 kV, 0.5 nA and 30 kV, 0.3 nA, and polishing at 5 kV. The HRTEM imaging was collected by JEOL 2100F TEM, operating at a voltage of 200 kV. The HAADF-STEM was done in an ARM200CF microscope, operating at 200 kV with aberration correction on the probe giving a probe size of less than 0.1 nm.

We have studied optical properties of the grown BAs layers using cathodoluminescence (CL) at two independent facilities. At Loughborough, optical properties were studied using cathodoluminescence in a pFIB/SEM—Helios G4 pFIB (Thermo Fisher Scientific) system, equipped with CL Gatan monarc Pro CL system PMT (185–980 nm) CCD (185–1100 nm). Due to the low thickness of the deposited BAs layers, an accelerating voltage of 1 keV and a current of 1.6 nA were used to collect the CL data. Spectra were collected on the CCD using a 300 nm grating blazed at 600 nm, a slit width of 15 nm, and 5 s frame averaged collection time was used. The spectra have not been adjusted to account for the quantum efficiency of the camera or mirror as these corrections can introduce artifacts at long wavelengths.

CL was also measured in Strathclyde at low beam energies (1–3 kV) using a customized field-emission SEM (FEI Quanta 250FEG). The sample is inclined at approximately 45° toward this detector.[29] The light is focused to the 50 μm entrance slit of a 1/8 m spectrograph (Oriel MS125), in which it is dispersed with a 1200 lines mm^{-1} grating and detected using a charge-coupled device (Andor Technology Newton EMCCD). The spectra were background corrected using a spectrum acquired with the electron beam blanked and were also corrected for the system response.

Out of plane thermal conductivities were measured using nanosecond time-domain thermoreflectance (ns-TDTR). Samples were coated with an evaporated 150 nm-thick gold (Au) transducer layer and a 10 nm-thick chromium (Cr) adhesion layer. In the TDTR measurements, a 532 nm pulsed pump laser with a 3 ns pulse duration heated the sample surface, while a 491 nm continuous width probe laser monitored transient changes in reflectivity, which is proportional to temperature change. The effective pump and probe laser spot size was 13 μm. Thermal conductivity was extracted by fitting an analytical heat diffusion model, with further set up and method details provided earlier,[30] the measurements had little sensitivity to the in plane thermal conductivity. To minimize fitting parameters, a bare sapphire substrate was measured first, which became a fixed value in subsequent analysis of the BAs samples. The cross-plane thermal conductivity (κ) and thermal boundary resistance between the Au transducer and BAs were then fitted.

III. RESULTS AND DISCUSSION

We have grown BAs layers on 3C-SiC templates and sapphire substrates in the growth temperature range from ∼150 to ∼820 °C. Growth temperatures were measured using the substrate heater thermocouple. In all growth sets, we used a fixed boron cell temperature of 1850 °C and arsenic As_2 flux of $\sim 1.2 \times 10^{-6}$ Torr BEP. To prevent damage of the boron shutter at high source temperatures, we opened both B and As MBE shutters during boron cell heating and closed them during boron cell cooling when the boron cell temperature reached ∼1100 °C, with the substrate remaining at the designated epitaxial temperature. Therefore, the substrates were exposed to a fixed arsenic and increasing boron flux during the start of the growth and to arsenic and decreasing boron flux after the growth. The ramp rate for the boron cell was 10 °C/min. The layer growth time at the boron cell temperature of 1850 °C was fixed at 1 h. For all samples, the RHEED pattern from the substrate surface did not change up to a boron cell temperature of ~1700 °C. Therefore, we can conclude that, at these boron source temperatures, the concentration of boron atoms on the substrate surface remains low, and that arsenic is not strongly adsorbing to the surface of the substrate. When the boron cell reached ~1800 °C, the RHEED pattern started to change from the reconstructed 3C-SiC or sapphire surface patterns to diffuse concentric rings showing polycrystallinity and formation of amorphous layers. At cell temperatures above ~1800 °C, the boron flux becomes significant, which resulted in the formation of a boron-stabilized substrate surface and subsequent growth of the BAs layer.

The AFM images in Fig. 1 for growth on sapphire substrates show that the layers grown at substrate temperatures up to 640 °C are very flat and likely amorphous or polycrystalline with very small grain sizes. Increasing the growth temperature above 640 °C increased the size of the grains. The surface roughness also rapidly increased with increase of the growth temperature, as shown in Fig. 2. At the highest temperature of ~820 °C used, we observed strong clustering, with an exposed surface around the clusters that has a similar roughness to the layers grown at low temperatures (0.66 ± 0.14 nm).

Figure 3 shows a secondary electron image and a WDX surface composition map for boron in the sample grown at the highest temperature of ~820 °C. In this sample, we have observed clustering on the surface by AFM, as shown in Fig. 1(f). The WDX map clearly shows that boron distribution on the surface mirrors the shape and position of clusters in the SEM image in Fig. 2(a). We were not able to detect any arsenic on the surface within the sensitivity of WDX. Therefore, we can conclude that at these high temperatures ~820 °C and we have boron-rich clustering on the layer surface.

Figure 4 shows x-ray photoelectron spectra for layers grown on sapphire substrates at different temperatures. We can see XPS peaks for boron (B 1s at ~188 eV) and arsenic (As 3d at ~43 eV) for all samples. At high growth temperatures (≥700 °C), we also see the Al 2p peak of the sapphire substrate with increasing intensity. Given that we observe B-rich clustering on the surface at high growth temperatures by AFM and WDX [Figs. 1(f) and 3, respectively], we conclude that aluminum peak is from the sapphire substrate in thin regions between the boron clusters. Quantification of the XPS survey spectra indicates that the layers contain an excess of boron irrespective of the growth temperature. The total As:B ratio, shown in blue in Fig. 4(b), decreases monotonically from 0.60 ± 0.02 at 300 °C to an almost pure boron surface with As:B equal to 0.019 ± 0.001 at 820 °C. This can be explained by the small sticking coefficient of arsenic at high temperatures.

Close inspection of the high-resolution core level spectra in Fig. 5 reveals a more complex picture. At low growth temperatures, the B 1s core level contains a singular peak, as shown in Fig. 5(a), which we attribute to B–As bonding.[31] The As 3d core level, shown

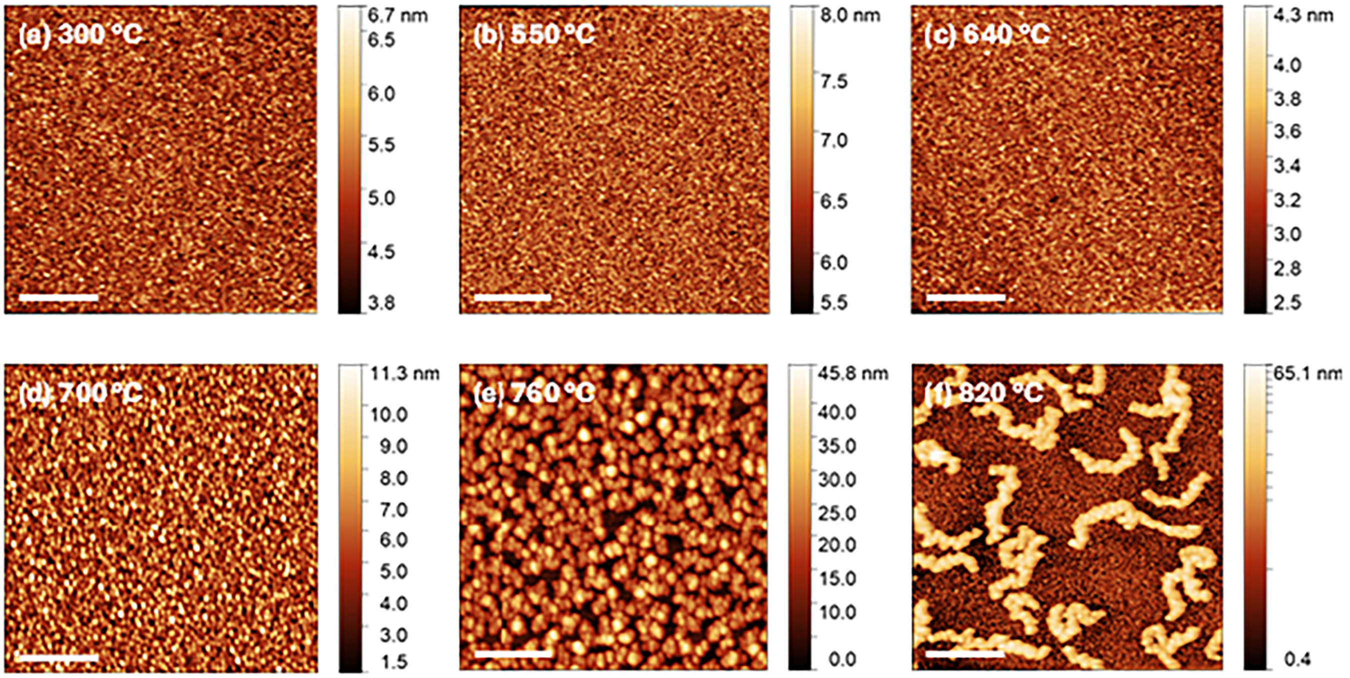

FIG. 1. AFM morphology of BAs layers grown on sapphire as a function of growth temperature: (a) 300, (b) 550, (c) 640, (d) 700, (e) 760, and (f) 820 °C. Scale bars are 500 nm.

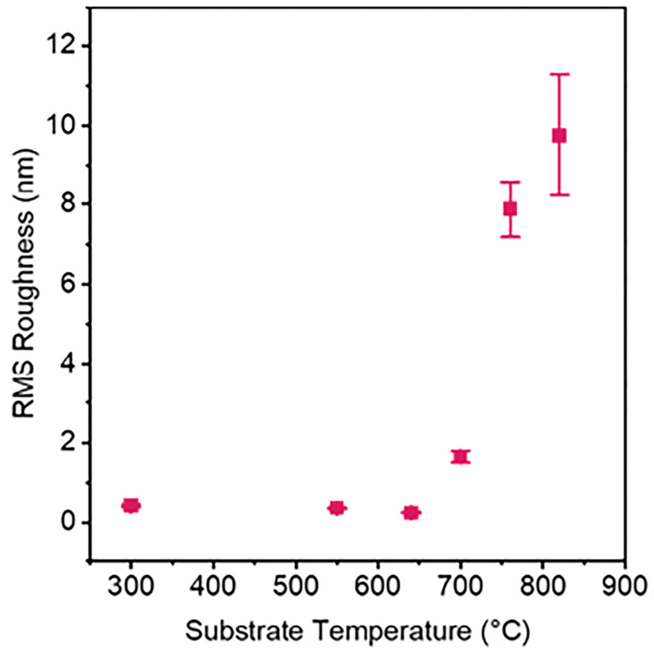

FIG. 2. Dependence of root mean square roughness of the BAs layer surface as a function of the growth temperature.

in Fig. 5(b), contains two components: a spin-split doublet at 42.30/42.98 eV, which is in agreement with B–As bonds,[31] and a doublet at 45.00/45.68 eV which is attributed to As_2O_3 (Ref. 32). The presence of arsenic oxide on the surface can be attributed to ambient oxidation of residual arsenic from the MBE growth chamber that deposits on the sample surface after growth during cooling. Considering this, the ratio of As:B in the grown layers is even lower, as shown in the red points in Fig. 4(b), ranging from 0.39 ± 0.02 at low temperatures to 0.009 ± 0.001 at high temperatures. As the growth temperature increases, we observe a gradual shift in the B 1s peak to lower binding energies toward the position of pure B, which we attribute to the reduced As content in the BAs_x matrix. We note that in the low-temperature regime (≤700 °C), it is not possible to resolve distinct chemical states in the B 1s core level [Figs. 5(a) and 5(c)], which suggests that the arsenic is distributed throughout the layer, rather than segregated into stoichiometric phases. At high growth temperatures (≥760 °C), we observe a splitting of the B 1s core level into two components [Fig. 5(e)] whose binding energies correspond to pure B and BAs components,[31,33] and the appearance of an additional doublet in the As 3d core level at 43.17/43.85 eV. The nature of these additional peaks is not well understood; however, given the de-wetting of boron and exposure of a thinner layer on the surface at high growth temperatures, we propose that these peaks originate from bonds at the sapphire/BAs interface.

Figure 6 shows SIMS depth profiles for B, As, C, and Si for a BAs layer grown on cubic 3C-SiC/Si templates. The growth temperature for this layer was ∼760 °C, and the thickness of the layer is about 27 nm based on ellipsometry results. Most of the boron was found at mass 11, confirming the isotopic purity of boron source material. To study boron in SIMS, we have used the dominant ^{11}B signal to study arsenic we have used the ^{75}As signal, with ^{13}C and ^{30}Si for the SiC substrate. All signals were not quantified and are presented in arbitrary units. As our BAs layers are relatively thin, we can only estimate the position of the BAs/SiC interface in Fig. 6 by the drop of the B- and As-containing signals and the increase of the Si and C signals. We observed a gradual decrease in the SIMS signals for B- and As-containing ions in the BAs layer. This is not due to diffusion of B and As into the SiC substrate but is a SIMS

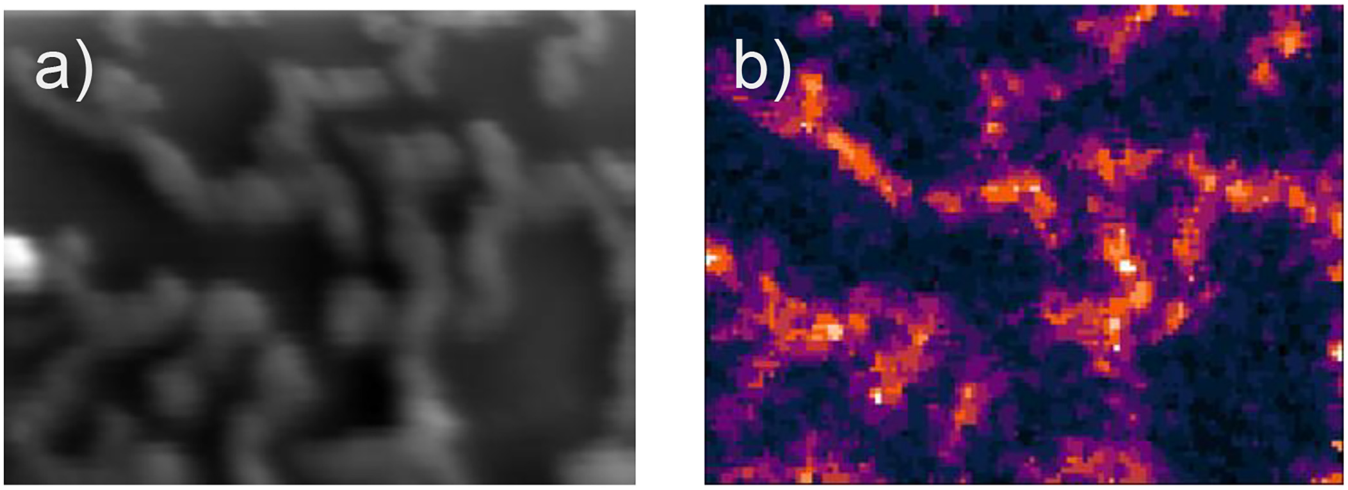

FIG. 3. Secondary electron microscopy image (a) and WDX map for the intensity of boron signal (brightest strongest) (b) in the 2.0 × 1.5 μm^2 surface area for the layer grown at the highest temperature ∼820 °C. The WDX region was mapped at 5 kV, 1 nA for ∼50 min.

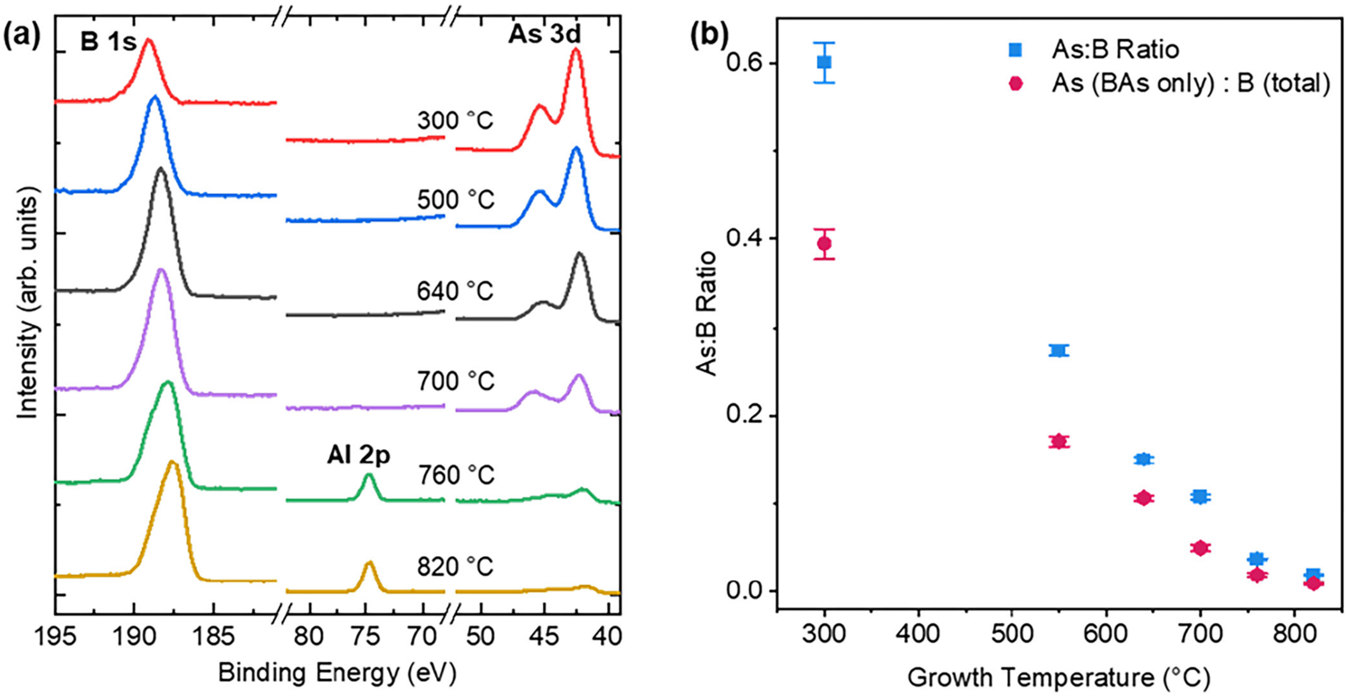

FIG. 4. (a) XPS spectra from BAs layers as a function of growth temperature. (b) As:B ratio of the layers as a function of BAs growth temperature. The blue squares consider the total boron and arsenic content of the layer, whereas the red circles used only the proportion of the As 3d core level that has been assigned to BAs (see Fig. 5).

artifact due to roughening of the crater during sputtering. Figure 6 clearly demonstrates incorporation of As in the BAs layer grown at temperatures of ∼760 °C. Currently, we are not able to draw any conclusions from SIMS about the stoichiometry of the BAs layers due to the lack of boron and arsenic SIMS calibration standards in such a matrix.

This temperature of ∼760 °C is significantly higher than normal temperatures for the MBE growth of GaAs layers[22,34] of about 500–600 °C, so the chemistry of reaction between boron and arsenic for BAs growth and gallium and arsenic for GaAs epitaxial MBE process must be significantly different.

There are studies by MOCVD and MBE to incorporate boron into GaAs to form dilute-boride $B_xGa_{1-x}As$ alloys.[35–39] The growth temperatures in these studies remain below 670 °C with maximum incorporation of boron up to 15%. However, the growth kinetics of these dilute-boride $B_xGa_{1-x}As$ alloys are dominated by reaction between Ga and As and, therefore, are similar to epitaxy of GaAs. In the case of boron arsenide MBE, we have only boron and arsenic fluxes coming to the growth surface, and the reactions between them seem to be completely different.

We used VASE to analyze the optical properties of the layers. At each growth temperature, the optical dispersion and thickness of the grown layer was determined. To compare sample properties, the refractive index of the layer at a photon energy of 2 eV was chosen as this is at an energy below the energy at which the refractive index is a maximum. The refractive index at 2 eV is essentially constant, within the significant measurement uncertainties, up to a growth temperature of 640 °C, as shown in Fig. 7. At higher growth temperatures, the refractive index decreases significantly as the temperature increases reflecting a significant change in optical properties and, therefore, stoichiometry of BAs films grown at temperatures of 640 °C and above.

Figure 8 presents the dependence of the thickness of BAs layers on the growth temperature in the range 300–820 °C. The thicknesses of the layers were estimated by variable angle spectroscopic ellipsometry, as discussed above. In all MBE experiments, we have used the same boron and arsenic fluxes during growth and the same growth time, the only variable parameter was the substrate temperature. We observed a gradual increase in the measured layer thickness with decreasing epitaxial temperatures from ∼640 to 300 °C. We attributed this increase to arsenic accumulation on the surface at low temperatures. The adsorption of arsenic to the layer surface gradually increased with decrease in temperature, as also confirmed by XPS results on Fig. 4. At the lowest temperatures, we even observed clustering of arsenic on the layer surface. We observed an unexpected increase of the layer thickness as the growth temperature increased from 640 to 750 °C. We have grown an additional set of the BAs layers at the high-temperature range to confirm the initial data, indicated by the red line in Fig. 8. This second set confirmed that this result to be reproducible. We observed an abrupt drop in the thickness of the layer grown at the highest temperature of ∼820 °C, likely due to boron clustering at

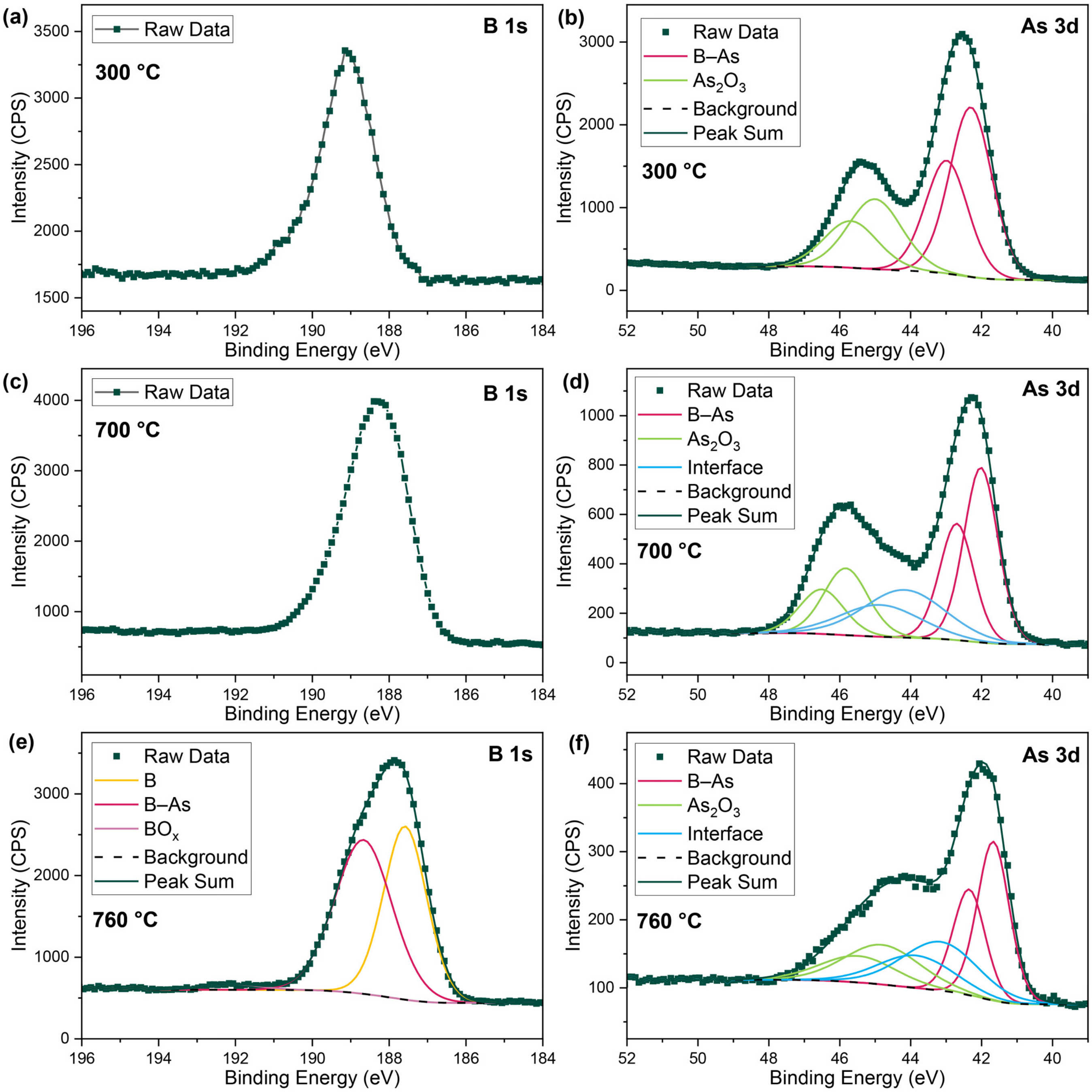

FIG. 5. High-resolution B 1s and As 3p core level spectra for BAs layers at different growth temperatures of (a) and (b) 300, (c) and (d) 700, and (e) and (f) 760 °C.

this high epitaxial temperature, as shown in Figs. 1(d) and 3. Such an increase in the thickness at high growth temperatures is consistent with the theoretical prediction that formation of BAs becomes endothermic above temperature of 1000 K (727 °C),[20] and arsenic began actively adsorbing, reacting, and to incorporate in the boron-stabilized layer surface. However, at temperatures above 800 °C, we started to observe a boron clustering, as shown in Figs. 1 and 3. Clustering results in a decrease in the arsenic incorporation, as

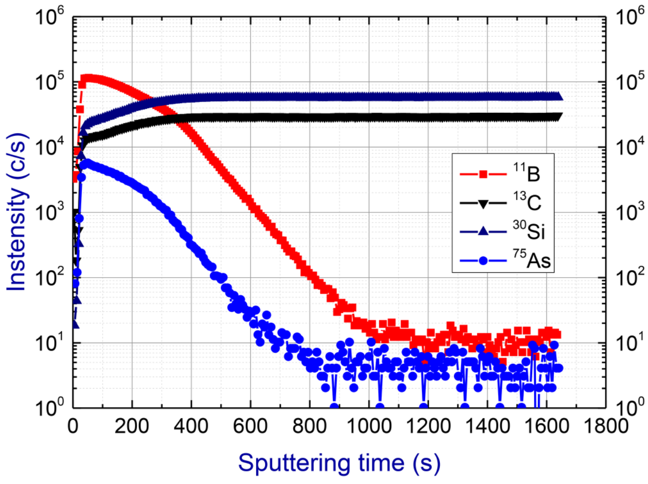

FIG. 6. SIMS depth profiles for B, As, C, and Si for a BAs layer grown on cubic 3C-SiC/Si templates.

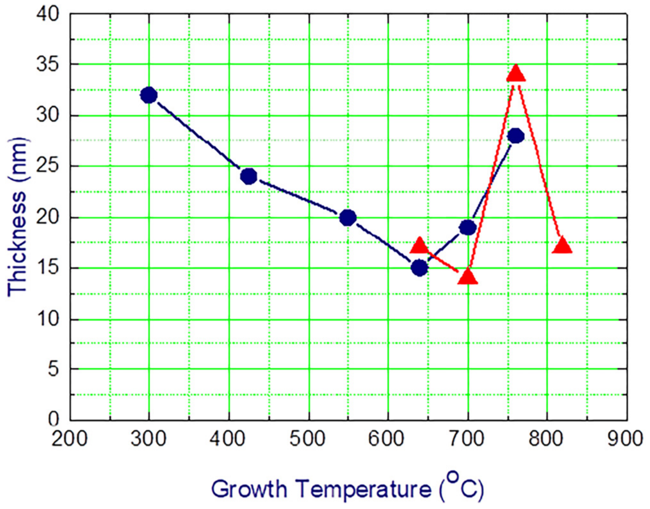

FIG. 8. Thickness of boron arsenide layers as a function of the growth temperature. All films were grown using the same boron and arsenic fluxes and the same growth time. Blue dots—initial growth set and red triangles—second high-temperature growth set.

demonstrated by WDX results in Fig. 3. This temperature range, 720–800 °C, is matching the optimum temperatures for successful CVT growth of BAs microcrystals.[21] Therefore, it is possible that these high epitaxial temperatures are beneficial for chemical reactions between arsenic and boron atoms at the growth surface with the formation of BAs.

Figure 9 shows high-resolution cross-sectional images of the BAs/sapphire interface area taken by STEM in high angle dark-field using an annular detector with inner and outer radii of 73 and 236 mrad [Fig. 9(a)] and high-resolution TEM [Fig. 9(b)], viewed approximately along the [10–10] sapphire direction (m axis). In the HAADF-STEM image, intensity is dominated by incoherently scattered electrons due to Rutherford scattering from the nucleus, giving contrast which is Z (atomic number) and thickness dependent, varying roughly as Z^2 ($Z^{(1.6–1.7)}$ in practice).[40,41] The relatively dark band (~0.5 nm) adjacent to the sapphire surface suggests materials of lower atomic numbers than the average in the sapphire substrate and later BAs layers. This could be explained by a layer near the epilayer/substrate interface being relatively high in B content at the start of growth, and with the As content increasing in the later growth to form BAs with a better stoichiometry, consistent with observations reported above.

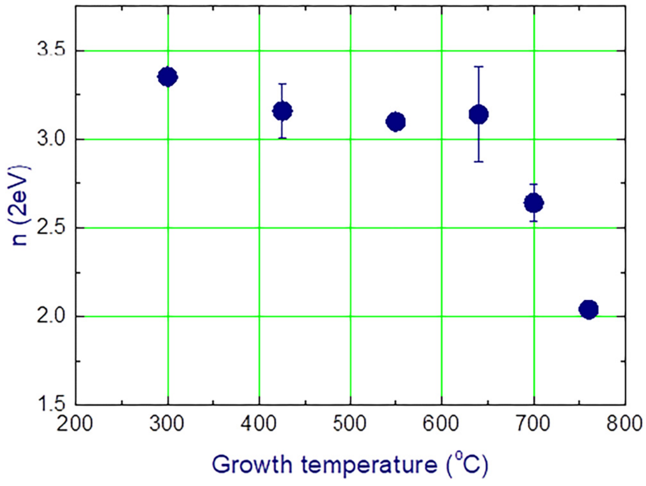

FIG. 7. Refractive index of boron arsenide (BAs) films at 2 eV as a function of growth temperature.

In contrast to the STEM images which are taken with a highly convergent electron beam, the TEM image in Fig. 9(b) is taken with a parallel beam, with contrast dominated by strong coherent Bragg scattering from the edge-on lattice planes. Although intensity is now no longer simply related to atomic number [i.e., the dark band zoomed in at the BAs/sapphire interface in Fig. 9(b) is probably, but not conclusively the low-Z layer seen in HAADF], significantly, the Bragg scattering highlights evidence for at least two distinct edge-on atomic layers [as shown in the right inset in Fig. 9(b)] at the onset of BAs growth with a separation of approximately 2.55 ± 0.33 Å. This has been calibrated by the spacing of 4.33 Å for the c/3 planes in the sapphire, where c = 12.99 Å. Further into the BAs layer, the structure appears amorphous. If we assume that cubic BAs is present, it is possible that initial growth is that of (111) BAs layers, matching the hexagonal symmetry of the sapphire surface.[42] In this case, the layer spacing would be 2.76 Å($a\sqrt{3}$) assuming $a = 4.78$ Å.[9] Therefore, in the initial growth phase, the cubic BAs layer might align with the hexagonal structure of the sapphire substrate and grow in the ⟨111⟩ direction for a few crystalline monolayers, however, after that BAs becomes amorphous.

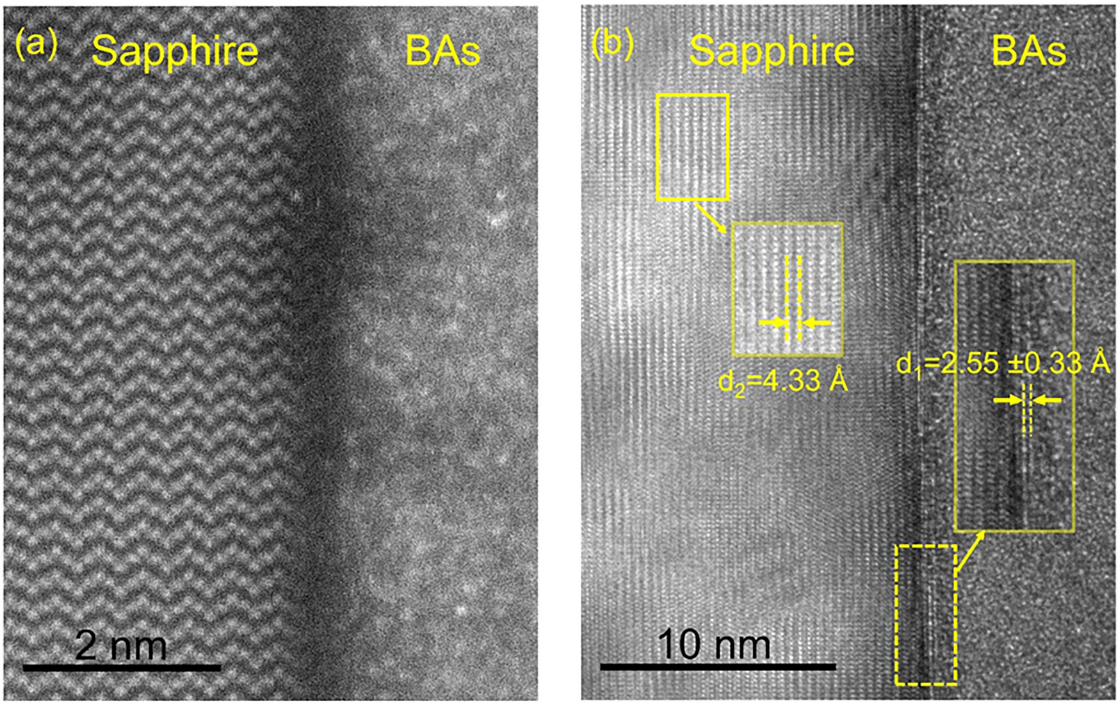

FIG. 9. Electron microscopy image of the BAs layer grown at 760 °C on the sapphire substrate viewed approximately along the [10–10] sapphire direction (m axis). (a) Scanning transmission electron micrograph depicting HAADF-STEM image. (b) HRTEM image. The two insets show the details of two distinct edge-on atomic layers at the BAs/sapphire interface area and the adjacent sapphire lattice. AFM morphology of BAs layers grown on sapphire as a function of growth temperature.

We have studied optical properties of the grown BAs layers using low beam voltage cathodoluminescence at two independent CL facilities in Loughborough and Strathclyde. CL of thin films is typically performed with accelerating voltages of 3–5 keV. At such voltages on clean sapphire substrates, we reproducibly detected a strong CL peak at ∼653 nm (∼1.89 eV), as shown in Fig. 10. Initially, these acceleration voltages were also used to study CL in our BAs layers, but the spectra were dominated by the CL from the sapphire substrate.

We were able to reproducibly detect a CL peak from our BAs layers at low accelerating voltages of 1–2 keV, as shown in Figs. 10 and 11. The low CL voltages are required due to the nanometer thinness of the grown BAs layers, as shown in Fig. 8. The strong CL peak is broad and centered at about ∼735 nm (∼1.67 eV). The position of the peak at ∼1.67 eV is consistent with published experimental and theoretical data with reported values for BAs an indirect gap of 1.674 eV and a direct gap of 3.990 eV (please see report of Ref. 43 and reference therein). Our layers have a thickness of a few tens of nanometers, and, therefore, we still detect a high-energy CL peak from sapphire at ∼653 nm (∼1.89 eV) as a shoulder in the CL emission from BAs, as shown in Figs. 10 and 11.

As a control experiment, we have also grown pure boron layers on both types of substrates without an intentional arsenic flux under the identical MBE conditions. The intensity of the CL peak from the pure boron layer grown at the same temperature is several orders of magnitude weaker, as shown in Fig. 10. The fact that CL from pure boron is not completely zero suggests that it may be some reaction of MBE-background arsenic with boron during or after the epitaxy. The strong reproducible CL peak from the BAs layer in Fig. 10 strongly supports that we have observed the formation of BAs in the grown layer.

We reproducibly observed CL peak at ∼1.67 eV (∼735 nm) in our BAs layers at both CL facilities. The intensity of the CL peak strongly depends on the MBE conditions gradually increasing with an increase in the substrate growth temperatures, as shown in Fig. 11. The strongest intensity was observed in layers grown in the temperature range from 700 to 760 °C. Therefore, we can conclude that BAs layers grown at that high temperature range probably have a better structural quality.

The intensity of the CL peak at ∼1.67 eV from the BAs layers decreased with an increase in the growth time, probably due to lower structural quality of the thicker layers. The CL peaks are broad as a result of amorphous/polycrystalline structure with high point-defect density in our BAs layers. However, the position of the peak was not shifted with the thickness or growth time.

Figure 12 shows the thermal conductivity of the BAs layers, illustrating that thermal conductivity increases with a substrate growth temperature above 600 °C. The uncertainty of the layer thickness is reflected in the error bar displayed. The increase in uncertainty at higher thermal conductivity reflecting the shorter

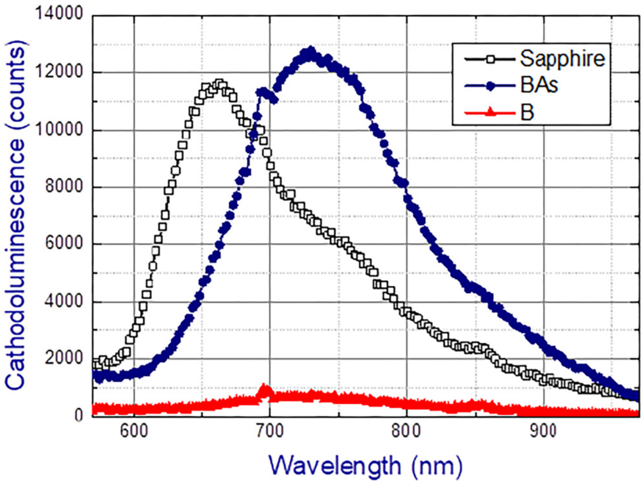

FIG. 10. Cathodoluminescence from the clean sapphire substrate, boron (B), and BAs layers grown at 760 °C. For BA CL studies, an accelerating voltage of 1 keV and a beam current of 1.6 nA were used.

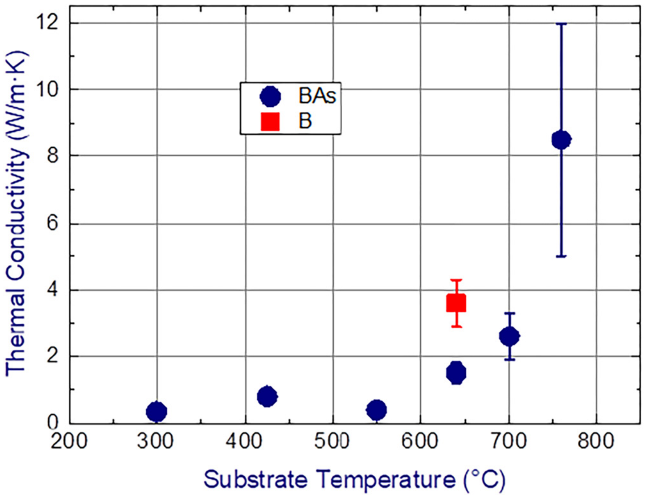

FIG. 12. ns-TDTR obtained thermal conductivity for BAs and boron (B) layers grown at different temperatures on sapphire.

diffusion time of the heat transfer through the thin layer reduces our measurement sensitivity to the BAs layer. The specific heat capacity and density for BAs and sapphire were 402 J/kg K, 5220 kg/m^3[41] and 778 J/kg K and 3980 kg/m^3,[30] respectively, which does not affect the fitting significantly. The observed thermal conductivity in Fig. 12 is significant below 900–1300 W/m K, reported for single-crystalline BAs,[9–11] illustrating the impact of grain boundaries and point devices, apparent in the TEM images of Fig. 9, though increasing the growth temperature illustrate the improving quality of the films. Therefore, to further improve the thermal conductivity, we must improve the stoichiometry to significantly decrease the defect density concentrations.[9–11]

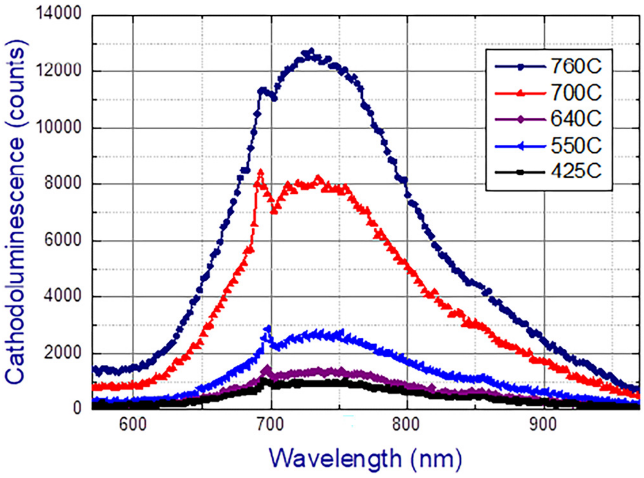

FIG. 11. Cathodoluminescence from BAs layers grown at different temperatures, an accelerating voltage of 1 keV and a beam current of 1.6 nA were used.

IV. SUMMARY AND CONCLUSIONS

We have grown boron arsenide layers by MBE on 3C-SiC/Si and sapphire substrates in a wide temperature range from 150 to 820 °C. At the highest temperature of ~820 °C, strong boron clustering on the surface was observed by AFM and WDX. At lower growth temperatures, we have confirmed incorporation of arsenic to the grown layers by XPS, SIMS, and TEM techniques. The best quality of the boron arsenide layers was achieved at a high growth temperature range around 750 °C. Thicknesses and roughness of the BAs layers increase for epitaxy above 600 °C. Refractive index of boron arsenide falls significantly for epitaxy above 600 °C suggesting a significant change in optical properties and stoichiometry. TEM data demonstrate that high temperature nucleation of the layer started with the deposition of boron-rich monolayers on the substrate surface. STEM data for the epitaxy on sapphire show that in the initial growth phase, the cubic boron arsenide layer aligns with the hexagonal structure of the sapphire substrate and grows in the ⟨111⟩ direction for a few crystalline monolayers; however, currently, we are not able to sustain that and the layer becomes amorphous. For boron arsenide layers grown at high temperatures, we have observed an increase in the thermal conductivity and cathodoluminescence emission with a reproducible CL peak centered at ~1.67 eV, confirming the formation of the boron arsenide material in the layers. The experimental results are explained by increased chemical interaction between arsenic and boron at temperatures above ~600 °C. Boron arsenide layers currently remain amorphous/polycrystalline and contain an excess of boron. We probably may use B_xAs_y instead of BAs to demonstrate that stoichiometric control in grown layers remains a challenge. However, we decided to keep BAs through the text for simplicity. All our experimental data show that MBE growth conditions need to be optimized further first to improve stoichiometry and after that to decrease point-defect densities in the boron arsenide layers.

ACKNOWLEDGMENTS

This work at Nottingham and Bristol was supported by the Engineering and Physical Sciences Research Council UK (Grant Nos. EP/V05323X/1 and EP/W035510/1) and (Grant No. EP/W034751/1), respectively. We also acknowledge the University of Nottingham Propulsion Futures Beacon for funding toward this research. The authors acknowledge access to the National Facility for High Resolution CL Analysis of Photovoltaic and Optoelectronic Devices, funded by the EPSRC (Grant No. EP/X030245/1). We also want to acknowledge Loughborough Surface Analysis Ltd for SIMS measurements and discussions of results. The authors acknowledge use of characterization facilities within the David Cockayne Centre for Electron Microscopy, Department of Materials, University of Oxford, alongside financial support provided by the Henry Royce Institute (Grant Ref. No. EP/R010145/1). The authors acknowledge the Nanoscale and Microscale Research Centre (nmRC), University of Nottingham, for providing access to instrumentation, EPSRC Grant No. EP/K005138/1.

AUTHOR DECLARATIONS

Conflict of Interest

The authors have no conflicts to disclose.

Author Contributions

Tin S. Cheng: Conceptualization (equal); Data curation (equal); Formal analysis (equal); Investigation (equal); Methodology (equal); Writing – review & editing (equal). **Jonathan Bradford:** Conceptualization (equal); Data curation (equal); Formal analysis (equal); Investigation (equal); Methodology (equal); Writing – review & editing (equal). **Leo Norman:** Conceptualization (equal); Data curation (equal); Formal analysis (equal); Investigation (equal); Methodology (equal); Writing – review & editing (equal). **Xiaoyang Ji:** Conceptualization (equal); Data curation (equal); Formal analysis (equal); Investigation (equal); Methodology (equal); Writing – review & editing (equal). **Arpit Nandi:** Data curation (equal); Formal analysis (equal); Investigation (equal); Validation (equal); Writing – original draft (equal). **Gerardo T. Martinez:** Data curation (equal); Formal analysis (equal); Investigation (equal); Validation (equal); Writing – review & editing (equal). **Stuart Robertson:** Data curation (equal); Formal analysis (equal); Investigation (equal); Validation (equal); Writing – review & editing (equal). **Paul R. Edwards:** Data curation (equal); Formal analysis (equal); Investigation (equal); Validation (equal); Writing – review & editing (equal). **James W. Pomeroy:** Data curation (equal); Formal analysis (equal); Investigation (equal); Validation (equal); Writing – original draft (equal). **David Cherns:** Conceptualization (equal); Data curation (equal); Formal analysis (equal); Investigation (equal); Methodology (equal); Supervision (equal); Writing – review & editing (equal). **Christopher J. Mellor:** Conceptualization (equal); Data curation (equal); Formal analysis (equal); Investigation (equal); Methodology (equal); Supervision (equal); Writing – review & editing (equal). **Robert W. Martin:** Conceptualization (equal); Data curation (equal); Formal analysis (equal); Investigation (equal); Methodology (equal); Supervision (equal); Writing – original draft (equal). **Peter H. Beton:** Conceptualization (equal); Data curation (equal); Formal analysis (equal); Investigation (equal); Methodology (equal); Supervision (equal); Writing – original draft (equal). **Martin Kuball:** Conceptualization (equal); Data curation (equal); Formal analysis (equal); Funding acquisition (equal); Investigation (equal); Methodology (equal); Project administration (equal); Resources (equal); Supervision (equal); Visualization (equal); Writing – original draft (equal); Writing – review & editing (equal). **Sergei V. Novikov:** Conceptualization (equal); Data curation (equal); Formal analysis (equal); Funding acquisition (equal); Investigation (equal); Methodology (equal); Project administration (equal); Resources (equal); Supervision (equal); Validation (equal); Visualization (equal); Writing – original draft (equal); Writing – review & editing (equal).

DATA AVAILABILITY

The data that support the findings of this study are available from the corresponding author upon reasonable request.

REFERENCES

[1] C. Dames, Science **361**, 549 (2018).
[2] T. R. Anthony, W. F. Banholzer, J. F. Fleischer, L. Wei, P. K. Kuo, R. L. Thomas, and R. W. Pryor, Phys. Rev. B **42**, 1104 (1990).
[3] C. J. H. Wort and R. S. Balmer, Mater. Today **11**, 22 (2008).
[4] D. R. Lide, *CRC Handbook of Chemistry and Physics*, 77th ed. (CRC, Boca Raton, FL, 1996–1997).
[5] G. A. Slack, J. Phys. Chem. Solids **34**, 321 (1973).
[6] L. Lindsay, D. A. Broido, and T. L. Reinecke, Phys. Rev. Lett. **111**, 025901 (2013).
[7] T. Feng, L. Lindsay, and X. Ruan, Phys. Rev. B **96**, 161201 (2017).
[8] B. Lv *et al.*, Appl. Phys. Lett. **106**, 074105 (2015).
[9] J. S. Kang, M. Li, H. Wu, H. Nguyen, and Y. Hu, Science **361**, 575 (2018).
[10] S. Li, Q. Zheng, Y. Lv, X. Liu, X. Wang, P. Y. Huang, D. G. Cahill, and B. Lv, Science **361**, 579 (2018).
[11] F. Tian *et al.*, Science **361**, 582 (2018).
[12] J. S. Kang, M. Li, H. Wu, H. Nguyen, T. Aoki, and Y. Hu, Nat. Electron. **4**, 416 (2021).
[13] T. H. Liu, B. Song, L. Meroueh, Z. Ding, Q. Song, J. Zhou, M. Li, and G. Chen, Phys. Rev. B **98**, 081203 (2018).
[14] T. L. Chu and A. E. Hyslop, J. Appl. Phys. **43**, 276 (1972).
[15] Y. Gong, M. Tapajna, S. Bakalova, Y. Zhang, J. H. Edgar, Y. Zhang, M. Dudley, M. Hopkins, and M. Kuball, Appl. Phys. Lett. **96**, 223506 (2010).
[16] Y. Gong, Y. Zhang, M. Dudley, Y. Zhang, J. H. Edgar, P. J. Heard, and M. Kuball, J. Appl. Phys. **108**, 084906 (2010).
[17] Y. Zhang *et al.*, J. Cryst. Growth **352**, 3 (2012).
[18] J. A. Perri, S. La Placa, and B. Post, Acta Crystallogr. **11**, 310 (1958).
[19] T. L. Chu and A. E. Hyslop, J. Electrochem. Soc. **121**, 412 (1974).
[20] H. Dumont and Y. Monteil, J. Cryst. Growth **290**, 410 (2006).
[21] F. Tian and Z. Ren, Angew. Chem. Int. Ed. **58**, 5824 (2019).
[22] C. T. Foxon and B. A. Joyce, "Fundamental aspects of molecular beam epitaxy," in *Current Topics in Materials Science*, edited by E. Kaldis (North Holland, Amsterdam, 1981), Vol. 7.
[23] Y. J. Cho *et al.*, Sci. Rep. **6**, 34474 (2016).
[24] T. S. Cheng, A. Summerfield, C. J. Mellor, A. Davies, A. N. Khlobystov, L. Eaves, C. T. Foxon, P. H. Beton, and S. V. Novikov, J. Vac. Sci. Technol. B **36**, 02D103 (2018).

[25] T. S. Cheng, A. Summerfield, C. J. Mellor, A. N. Khlobystov, L. Eaves, C. T. Foxon, P. H. Beton, and S. V. Novikov, Materials **11**, 1119 (2018).
[26] A. Summerfield *et al.*, Nano Lett. **18**, 4241 (2018).
[27] D. Nečas and P. Klapetek, Cent. Eur. J. Phys. **10**, 181 (2012).
[28] N. Fairley *et al.*, Appl. Surf. Sci. Adv. **5**, 100112 (2021).
[29] P. R. Edwards, L. K. Jagadamma, J. Bruckbauer, C. Liu, P. Shields, D. Allsopp, T. Wang, and R. W. Martin, Microsc. Microanal. **18**, 1212 (2012).
[30] C. Yuan, J. W. Pomeroy, and M. Kuball, Appl. Phys. Lett. **113**, 102101 (2018).
[31] U. Choudhry *et al.*, Matter **6**, 206 (2023).
[32] M. Fantauzzi, D. Atzei, B. Elsener, P. Lattanzi, and A. Rossi, Surf. Interface Anal. **38**, 922 (2006).
[33] C. W. Ong, H. Huang, B. Zheng, R. W. M. Kwok, Y. Y. Hui, and W. M. Lau, J. Appl. Phys. **95**, 3527 (2004).
[34] J. Orton and T. Foxon, *Molecular Beam Epitaxy: A Short History* (Oxford University, Oxford, 2015).
[35] M. Groenert, R. Averbeck, W. Hösler, M. Schuster, and H. Riechert, J. Cryst. Growth **264**, 123 (2004).
[36] A. J. Ptak, D. A. Beaton, and A. Mascarenhas, J. Cryst. Growth **351**, 122 (2012).
[37] J. F. Geisz, D. J. Friedman, S. Kurtz, J. M. Olson, A. B. Swartzlander, R. C. Reedy, and A. G. Norman, J. Cryst. Growth **225**, 372 (2001).
[38] H. Detz, D. MacFarland, T. Zederbauer, S. Lancaster, A. M. Andrews, W. Schrenk, and G. Strasser, J. Cryst. Growth **477**, 77 (2017).
[39] K. M. McNicholas, R. H. El-Jaroudi, and S. R. Bank, Cryst. Growth Des. **21**, 6076 (2021).
[40] K. Sohlberg, T. J. Pennycook, W. Zhou, and S. J. Pennycook, Phys. Chem. Chem. Phys. **17**, 3982 (2015).
[41] Z. W. Wang and R. E. Palmer, J. Phys. Conf. Ser. **371**, 012010 (2012).
[42] Y. Sun, Y. Niu, L. Zhang, J. Zhang, and R. Quhe, Appl. Phys. Lett. **125**, 082101 (2024).
[43] J. Buckeridge and D. O. Scanlon, Phys. Rev. Mater. **3**, 051601(R) (2019).